European Journal of Pharmaceutical Sciences 122 (2018) 94–104

Contents lists available at ScienceDirect

European Journal of Pharmaceutical Sciences

journal homepage: www.elsevier.com/locate/ejps

Design and characterization of loratadine nanosuspension prepared by ultrasonic-assisted precipitation

Areen Alshweiat, Gábor Katona, Ildikó Csóka*, Rita Ambrus

Faculty of Pharmacy, Institute of Pharmaceutical Technology and Regulatory Affairs, University of Szeged, Szeged, Hungary

ARTICLE INFO

Keywords:
Loratadine nanosuspension
Antisolvent precipitation
Sonication
Process parameters
Material parameters
Dissolution profile
Stabilization

ABSTRACT

Nanoparticle engineering is a well-defined technique employed as a novel and effective method in drug design and delivery. It is widely used to control particle size, as well as the morphological and physicochemical properties of active pharmaceutical ingredients. Furthermore, it serves as a method of pre-dispersion preparation for various dosage form developments. Nanotechnology produces nanomaterials with enhanced properties in terms of solubility, dissolution and permeability. In this work, ultrasonic-assisted precipitation was employed to produce nanosuspensions of poorly water-soluble loratadine, using different stabilizers. The objective of our study was attempting to prepare solid nanoparticles of loratadine to be used as a possible intermediate for designing various dosage forms. The effects of the type(s) and concentration(s) of stabilizer(s) on mean particle size were assessed. Optimal process parameters required to produce homogeneous nanoparticles with particle size below 500 nm and polydispersity less than 0.3 were determined both for precipitation and ultrasonication. Pre-dispersions were evaluated for their particle size, polydispersity index and zeta potential. Freeze-drying was employed to produce dry nanoparticles. Particle size, particle size distribution and zeta potential of the dried nanoparticles were measured after reconstitution in water. Besides thermal analysis using DSC and structural analyses (XRPD and FT-IR), the morphological characteristics and dissolution behaviors were also investigated. The selected freeze-dried nanoparticles had a mean particle size range of 353–441 nm, a polydispersity index ranging between 0.167 and 0.229 and a zeta potential between −25.7 and −20.7 mV. These results suggest that material and process parameters were successfully optimized. DSC and XRPD spectra confirmed interactions between the formulation's components during freeze-drying. The solid nanoparticles showed 30–42% of cumulative release after 10 min compared to less than 1% of dissolution characterizing loratadine without pre-processing. This study demonstrates that preparing dried loratadine nanoparticles suitable for designing effective drug preparations is a feasible approach.

1. Introduction

Nanotechnology is one of the most widely used approaches to overcome the inconveniences of solubility and poor bioavailability, as well as a method utilized to produce intermediate compounds for different dosage forms. Nanosuspensions have numerous outstanding advantages, including enhanced solubility and dissolution rate of otherwise poorly water-soluble drug compounds, high adhesiveness to biological surfaces, as well as easy formulation and scale up. Also, they allow reaching high drug concentrations and applicability in any types of drug formulations, such as preparations for oral, parenteral, dermal, pulmonary, ocular and nasal delivery (Bartos et al., 2015a; Chen et al., 2015; Merisko-Liversidge and Liversidge, 2008; Patravale et al., 2004; Pawar et al., 2014).

Nanosuspensions are colloidal dispersions of drug particles in the submicron size (mean particle size less than 1 μm) and need to be stabilized by a minimum amount of suitable ionic or/and steric stabilizer. The drug compounds (active pharmaceutical ingredients, APIs) included in nanosuspensions can exist in crystalline or amorphous forms. The produced liquid pre-dispersion can be converted into intermediate solid products, such as powder, by means of drying or into a semi-solid formulation, such as gel (Bartos et al., 2016; Hao et al., 2015; Lindfors et al., 2007; Rabinow, 2004).

Top-down and bottom-up procedures are generally applied for the preparation of nanosuspensions. The top-down approach includes comminution of large particles into nanoparticles, while the bottom-up approach employs the precipitation of nanoparticles from dissolved drug molecules. Although the top-down method is preferred in the pharmaceutical industry, the bottom-up method has the potential for producing homogenous nanoparticles with lower energy input

* Corresponding author.
E-mail address: csoka@pharm.u-szeged.hu (I. Csóka).

https://doi.org/10.1016/j.ejps.2018.06.010
Received 9 February 2018; Received in revised form 18 May 2018; Accepted 12 June 2018
Available online 14 June 2018

(Agrawal and Patel, 2011; Du et al., 2015; Iurian et al., 2017; Möschwitzer, 2010; Müller et al., 2011; Rahim et al., 2017).

Antisolvent precipitation is the most common and effective bottom-up technique currently applied in nanosuspension preparation. Its advantages include simplicity and cost-effectiveness. The method of antisolvent precipitation is based on the principle that a compound's solubility in a water-miscible organic solvent can be modified by adding an antisolvent which promotes precipitation. During precipitation, stabilizers dissolved in the antisolvent get absorbed on the crystal surfaces to inhibit further crystal growth (Ambrus et al., 2009; Matteucci et al., 2006).

Ultrasonication has been introduced as an effective method to be combined with precipitation to achieve an enhanced particle size reduction and to control the processes of nucleation and crystallization. When applied on liquid, ultrasound waves are characterized by a cyclic succession of expansion and compression phases, with compression cycles exerting a positive pressure and pushing the liquid molecules together, while expansion cycles exert a negative pressure and pull the molecules apart. Besides, ultrasound waves intensify mass transfer by initiating cavitation. Cavitational bubbles are formed during the negative-pressure phase. The phenomena of the formation, growth and subsequent collapse of microbubbles release a large magnitude of energy. When a bubble collapses, a confined hot spot with high temperature and pressure is formed, releasing powerful shock waves. Thus, mixing of the solvent and the antisolvent is enhanced, leading supersaturation of the mixture. Furthermore, the implosion of vacuum bubbles breaks down particles. The final results of this process are dependent on sonication duration and intensity, on the sonotrode's length and depth of immersion, as well as on temperature (Anil et al., 2016; Bartos et al., 2015b; Dhumal et al., 2008; Jiang et al., 2012; Liu et al., 2012; Mishra et al., 2015; Wu et al., 2013; Xia et al., 2010; Zhang et al., 2006).

In terms of stability, liquid nanosuspensions are characterized by physical and chemical instability attributed to aggregation, agglomeration, Ostwald ripening and changes of the crystalline state (Lindfors et al., 2007). Thus, an immediate transformation of nanosuspensions into solid nanoparticles facilitates stability and allows processing to produce various dosage forms. Freeze-drying is one of the most widely used methods for drying nanosuspensions. However, even the freeze-drying process may induce stress, which in turn influences the physical stability of nanosuspensions. The stress evoked during the freezing and drying phases can destabilize the colloidal system. During freezing, a phase separation is experienced, yielding ice and a cryo-concentrated solution phase. This highly concentrated system may promote aggregation of the particles. Moreover, the crystallization of ice may produce a mechanical stress on the nanosized particles, also leading to their destabilization. On the other hand, the dehydration phase involves the removal of ice and unfrozen water which remained dissolved or adsorbed on the solid phase (Abdelwahed et al., 2006a, 2006b; Beirowski et al., 2011; Quintanar-Guerrero et al., 1998; Van Eerdenbrugh et al., 2008; Wu et al., 2011).

Consequently, numerous parameters play a significant role in the particle size and properties of nanosuspension-based freeze-dried nanoparticles, including drug concentration, type(s) and concentration(s) of stabilizer(s), solvent type and solvent to antisolvent ratio, as well as sonication and drying conditions and additives. Thus, nanosuspension preparation with ultrasonic-assisted precipitation and freeze-drying of these nanosuspensions are complex asks that require a careful selection of both process and material parameters.

Loratadine (LOR), a second-generation histamine H_1 receptor antagonist, is the most frequently prescribed antihistamine drug for the treatment of allergic conditions, such as rhinitis, urticaria and atopic dermatitis. Recent studies have also reported LOR as a safe and effective emergency therapy for the management of bone pain induced by granulocyte-colony stimulating factors (G-CSFs). It is reported that10 mg of LOR is effective against NSAID-resistant severe G-CSF-induced bone pain (Moore and Haroz, 2016; Romeo et al., 2015). The compound's properties classify LOR as a class II agent according to the biopharmaceutical classification system, characterized by poor water solubility (3.03 µg/ml) and high permeability (logP = 5). It is a weak base with a reported pKa value of 5.25 at 25 °C, responsible for its pH-dependent solubility, and consequent variability in bioavailability (Dagenais et al., 2009; Han et al., 2004; Popović et al., 2009). Various techniques have been applied to enhance the solubility and dissolution properties of LOR, including solid dispersion, inclusion with ß-cyclodextrin derivatives, micellar solubilization and self-microemulsifying systems. Other studies have also reported the preparation of a LOR in situ gel as niosomes, as well as a nanoparticle loaded thermosensitive in situ gel for nasal delivery(Frizon et al., 2013; Hin Teng et al., 2015; Li et al., 2015; Nacsa et al., 2008, 2009; Popović et al., 2009; Vyshnavi et al., 2015).

The present research is known to be the first work to utilize the ultrasonic-assisted antisolvent precipitation approach to prepare LOR nanosuspensions (LNs), using cellulose derivatives (i.e. hydroxylpropylmethylcellulose, HPMC), polyvinylpyrrolidone (PVP-K25), Poloxamer 188 (Pluronic F 68), polysorbate (Tween 80) and sodium lauryl sulfate (SLS) either as a single stabilizer or in combination. The effects of the type(s) and concentration(s) of the stabilizer(s) on mean particle size were investigated. The novelty of our research includes the preparation of a nanoscale LOR powder that can be used as an intermediate for designing different dosage forms.

2. Materials and methods

2.1. Materials

LOR was purchased from Teva Ltd. (Budapest, Hungary). Hydrophilic polymers; Polyvinylpyrrolidone K-25 (PVP-K25) was supplied by ISP Customer Service GmBH (Cologne, Germany) and hydroxypropylmethylcellulose E50LV (HPMC) was supplied by Colorcon (Budapest, Hungary). Pluronic F68, a synthetic tri-block copolymer, was purchased from BASF (Ludwigshafen, Germany). The non-ionic surfactant Tween 80 was supplied by Fluka Chemika (Buchs, Switzerland), the anionic surfactant sodium lauryl sulfate (SLS) was supplied by Molar Chemicals Ltd. (Budapest, Hungary), methanol was purchased from FreeHand Ltd. (Pecs, Hungary), ethanol was supplied by Spectrum-3D (Debrecen, Hungary), and D-(+)-trehalose (TRE) was supplied by Sigma-Aldrich (New York, USA). Water was purified by double distillation.

2.2. Methods

2.2.1. Preliminary studies with LOR: solubility tests

Excess drug amount was added into 5 ml of distilled water or phosphate buffer solution (PBS; pH 7.4), followed by shaking at 25 °C for 24 h. A sample was taken, filtered and the amount of dissolved LOR was measured spectrophotometrically (Unicam UV/VIS Spectrophotometer, Cambridge, UK). Solubility in other solvents was determined gravimetrically by adding an excess amount of LOR into 5 ml of different water-miscible solvents, such as ethanol, acetone and methanol. The drug-containing solution was stirred at 4000 rpm for 1 h at room temperature (25 °C), and then 1 ml of each solution was filtered into a drying dish. The filtrate was allowed to stand for solvent evaporation, and the residual mass was weighed on a daily basis, using an analytical balance (Mettler Toledo Ax 205, d = 0.01 mg) to make sure of the total removal of the solvent. Constant mass indicates the solubility in 1 ml of the solvent used.

2.2.2. Preparation of loratadine nanosuspension (LN)

After the preliminary studies, LNs were prepared using the precipitation-ultrasonication method. LOR was dissolved in ethanol according to its solubility, while the stabilizer(s) was (were) dissolved in

water. For stabilizer mixtures of Tween 80 or F68 plusPVP-K25, one of the stabilizers (F68, Tween 80) was added to the solvent phase, while the other one (PVP-K25) was added to the antisolvent phase. Both solutions were filtered through a 0.45 µm filter (FilterBio PES Syringe Filter, Labex Ltd., Budapest, Hungary). The fresh-made LOR solution was rapidly introduced into the cool antisolvent under sonication using a UP 200 s Ultrasonic processor (HielscheruUltrasonics GmbH, Germany) and different conditions in terms of energy power, sonication time and sonication temperature. The temperature of sonication was controlled (Julabo F32, JULABO GmbH, Germany). LNs were stirred at room temperature for 24 h to remove the organic solvent.

2.2.3. Preparation of dried loratadine nanoparticles (DLN)

As detailed before, dried nanoparticles are more preferable for their chemical and physical stability. Freeze-drying was performed in a Scanvac, CoolSafe 100-9 Pro type apparatus (LaboGeneApS, Lynge, Denmark) equipped with a 3-shelf sample holder unit, recessed into the drying chamber. Nanosuspensions were lyophilized with 5% w/v TRE. The process was controlled by a computer program (Scanlaf CTS16a02), temperature and pressure were recorded continuously. The drying chamber where the samples were frozen had a temperature range between −97 °C and −88 °C. The process parameters are shown in Table 1.

2.2.4. Preparation of physical mixtures

Physical mixtures (PMs) corresponding to the composition of the nanosuspensions were prepared as reference samples by blending LOR and F68 in 1.25:1 weight ratio for PM1 or LOR, F68 and PVP-K25in 1.25:1:1 weight ratio for PM2, in a Turbula mixer (Turbula System Schatz; Willy A. Bachofen AG Maschinenfabrik, Basel, Switzerland) using 60 rpm for 10 min.

2.2.5. Particle size and zeta potential characterization for LNs

The mean particle size (MPS), zeta potential (ZP) and polydispersity index (PDI) of LNs were measured by laser diffraction using a Malvern Nano ZS zetasizer (Malvern Instrument, UK), using water as the dispersant and setting there fractive index to 1.62.

2.2.6. Characterization of dried nanoparticles (DLN)

2.2.6.1. Scanning electron microscopy (SEM). Morphology of the LOR, PMs and DLNs particles were characterized by scanning electron microscopy (SEM) (Hitachi S4700, Hitachi Scientific Ltd., Tokyo, Japan) at 10 kV. The samples were coated with gold-palladium (90 s) using a sputter coater (Bio-Rad SC 502, VG Microtech, Uckfield, UK) and an electric potential of 2.0 kV at 10 mA for 10 min. Air pressure was set to 1.3–13.0 mPa.

2.2.6.2. X-ray powder diffraction (XRPD). The structures of lyophilized nanoparticles and raw materials were characterized using a BRUKER D8 Advance X-ray powder diffractometer (Bruker AXS GmbH, Karlsruhe, Germany) with Cu K λ_1 radiation (λ = 1.5406 Å) and a VÅNTEC-1 detector. Powder samples were scanned at 40 kV and 40 mA, with an angular range of 3° to 40° 2θ, at a step time of 0.1 s and a step size of 0.01°.The degree of crystallinity (crystallinity index, %Xc) was calculated based on the following formula, where A is the area under the whole curve and pure LOR was considered as 100% crystalline.

$$Xc = \frac{A_{crystalline}}{A_{crystalline} + A_{amorphous}} * 100 \quad (1)$$

2.2.6.3. Differential scanning calorimetry (DSC). Thermal analysis was carried out using a differential scanning calorimeter (Mettler Toledo DSC 821^e, Mettler Inc., Schwerzenbach, Switzerland). About 3–5 mg of powder was accurately weighed into DSC sample pans, which were hermetically sealed and lid pierced. An empty pan was used as a reference in an inert atmosphere under constant argon purge. The samples were analysed in the temperature range of 25–300 °C at a heating rate of 5 °C min^{-1}.

2.2.6.4. Fourier-transform infrared spectroscopy (FTIR). FT-IR spectra of raw materials and DLNs were obtained by a Fourier-transform infrared spectroscope (Thermo Nicolet AVATAR 330, USA) equipped with the GRAMS/AI ver. 7program. Samples were grounded and compressed into pastilles with 150 mg dry KBr. The pastilles were scanned 128 times at a resolution of 4 cm^{-1}in the wave number region 4000–400 cm^{-1}.

2.2.6.5. Saturation solubility. Saturation solubility of PMs and selected DLNs was investigated by adding excess amounts of the sample into 5 ml of water or PBS, pH 7.4 at 25 °C. Next the samples were filtered, and the drug concentrations in the filtrate were measured by UV spectroscopy at λ_{max} 248 nm.

2.2.6.6. Drug content and dissolution studies. LOR contents of the selected DLNs were determined by dissolving 10 mg of the sample in 50 ml of 0.1 N HCl. After stirring the solution with a magnetic stirrer (400 rpm) at room temperature for 24 h, it was filtered and analysed. The concentration was measured spectrophotometrically at 248 nm. The quantities of the samples were chosen after drug content determination, where the measured drug content was between 79 and 93% compared to the theoretical drug content. The modified paddle method (USP dissolution apparatus, type II Pharma Test, Hainburg, Germany) was used to characterize the dissolution rates of LOR, PMs and DLNs. 1.11 mg of pure LOR or DLN equivalent to 1.11 mg of LOR in 100 ml PBS, pH 7.4 was used. The paddles were rotated at 100 rpm at 37 °C. 5 ml aliquots were taken at 5, 10, 15, 30, 60, 90 and 120 min and were filtered. Concentrations of LOR were measured spectrophotometrically (Unicam UV/VIS Spectrophotometer, Cambridge, UK) at λ_{max} 248 nm. The calibration curve was taken in the concentration range of 2–20 µg/ml. The calibration curve was linear throughout the whole range tested, and was described by the equation A = 0.0388 conc (R^2 = 0.9997). The slope was 0.039. At the maximum absorption of LOR, no absorption was detected for the excipients we used. The limit of detection and the limit of quantification for LOR were 0.401 and 1.216 µg/ml, respectively. The aliquots taken were replaced. However, sink conditions were not maintained during the dissolution process due to the poor solubility of LOR.

2.2.7. Model-independent kinetics of dissolution profiles

Dissolution efficiency (DE) of the samples was determined by calculating the percentage of the ratio of the area up to time t divided by the area that described 100% dissolution at the same time (Khan, 1975).

$$\%DE = \frac{\int_0^t y\ X\ dt}{y_{100}\ X\ t} \times 100\% \quad (2)$$

Table 1
Freeze-drying parameters used for LNs.

Process	Time (h:min)	Chamber pressure (mbar)	Product temperature (°C)	Shelf temperature (°C)
Freezing	01:00	–	−39	−40
Primary	02:00		−40 to −39	−40
drying	05:20	0.01	−38to −33	−20
	06:45		−32 to −27	0
Secondary	18:00		−26 to −25	+10
drying	18:40	0.01	−25 to −24	+20
	27:30		−23 to −5	+30
	36:10		−4 to +4	+30

Relative dissolution (RD) with respect to the raw LOR at 60 min was calculated using the following formula:

$$RD\ 60\ min = \frac{\%DE60\ min}{\%DE\ 60\ \text{min}\ LOR} \quad (3)$$

The trapezoidal method was used to calculate the area under the curve (AUC). AUC is the sum of all trapezia:

$$AUC = \sum_{i=1}^{i=n} \frac{(t_1 - t_{i-1})(y_{i-1} + y_i)}{2} \quad (4)$$

where t_i represents the time point and y_i is the percentage of sample dissolved at time t_i. Mean dissolution time (MDT) was calculated as follows (Costa and Lobo, 2001):

$$MDT = \frac{\sum_{i-1}^{n} t_{mid}\,\Delta M}{\sum_{i-1}^{n} \Delta M} \quad (5)$$

where i is the dissolution sample number, n is the number of dissolution times, t_{mid} is the time at the midpoint between times t_i and t_{i-1} and ΔM is the amount of LOR dissolved (mg) between times t_i and t_{i-1}.

3. Results and discussion

3.1. Preliminary studies

3.1.1. Solubility of LOR in different solvents and selection of the optimal organic solvent

LOR showed poor solubility in water and PBS (2.21×10^{-3} and 4.88×10^{-4} mg/ml, respectively) On the contrary, it is freely soluble in organic solvents such as ethanol, methanol and acetone (662.8, 563.1 and 445.1 mg/ml, respectively). Based on our preliminary tests, ethanol was used as an organic solvent with high LOR solubility. It is water miscible with low viscosity which guarantees a higher diffusion rate and the formation of many nuclei, and thus a smaller particle size. Moreover, the higher solubility of the drug in the organic solvent is preferable for a higher drug concentration which supports supersaturation.

3.2. Selection of process parameters

To prepare nanoparticles, the proper design of the experiment is inevitable, so process parameters should be cautiously adjusted to support nanoscale production. In case of ultrasonic-assisted precipitation, both precipitation and sonication parameters need to be defined and selected in the light of the particle size. To optimize this process, the drug amount and the stabilizer's type and concentration were fixed at 100 mg and 0.2% w/v of F68, respectively, and different solvent: antisolvent ratios, sonication temperatures, sonication times and sonication powers were applied at fixed freeze-drying conditions (Fig. 1).

Using a solvent: antisolvent ratio of1:20 at fixed 50%, 4 °C, 30 min sonication amplitude, temperature and process length, respectively, we were unable to produce nanoparticles, because the stabilizer's concentration was too low to cover the newly formed surfaces, leading to crystal growth with an average particle size of 2.82 µm. On the other hand, solvent: antisolvent ratios of 1:40 and 1:60 under the same sonication conditions yielded nanoscale particles with approximately 246.5 ± 1.83and 238.6 ± 2.31 nm MPS, respectively.

Ultrasonic amplitudes of 50, 70, and 100% were applied at the 1:40 solvent/antisolvent ratio for 30 min and 4 °C. Particles size efficiently decreased to approximately 246 nm at 50% amplitude. However, no significant reduction was achieved with further increment, when MPS was at the order of 235 nm ± 4.45. On the other hand, the length of sonication had a crucial effect on particle size when the power and temperature of sonication were fixed at 50% and 4 °C, respectively. 10 min were too short to produce nanoparticles (MPS 1.103 µm), and 20 min produced unstable LNs with crystals precipitating immediately. A sonication time of 30 min was an appropriate sonication length to produce LNs. Sonication temperature affects particle size in a well-known manner: generally, the lower the temperature is, the smaller the crystals are. Reasonably, high temperature increases the drug's solubility with a consequent decrease of supersaturation and nuclei numbers. The other explanation for the temperature effect is related to a higher rate of diffusion and to the kinetic reaction at the crystal surface, resulting in increased crystal growth (Matteucci et al., 2006). For example, for nitrendipine, particle size was reduced from 4.43 µm to 211 nm when precipitation temperature was changed from 35 to 3 °C, and for carvedilol 221 nm MPS was yielded when sonication temperature was controlled at 4–8 °C (Liu et al., 2012). In our study, reducing temperature from 25 to 4 °C reduced particle size from 3.21 µm to the nanoscale when all other parameters were fixed.

The process parameters selected for F68 were used for the other stabilizers tested to evaluate the effect of stabilizer type on particle size of LNs. The requirements for producing nanoparticles with the lowest particle size and a PDI less than 0.3 were previously determined to ensure a homogenous particle size distribution.

3.3. Effects of material parameters on particle size and stability of LNs

To produce a stable nanosuspension, steric and/or electrostatic barriers must provide adequate wetting and effectively prevent the aggregation of particles. Furthermore, it is important to keep a uniform particle size to prevent Ostwald ripening (Rabinow, 2004). Table 2 shows MPS, PDI and ZP for pure LOR and for the prepared LNs. Mean particle size for unprocessed LOR was approximately 4.6 µm. Using

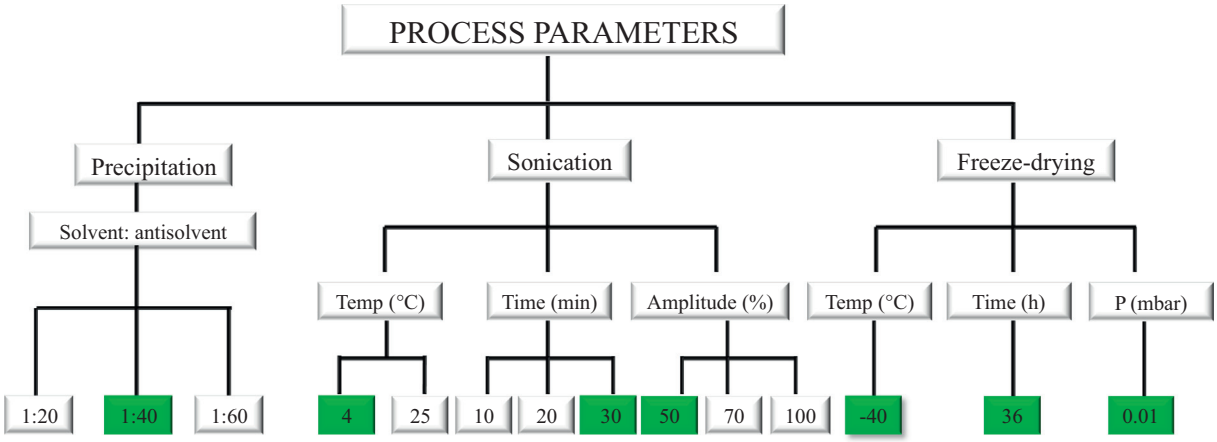

Fig. 1. Schematic diagram for the selection of process parameters.

Table 2
Mean particle size (MPS), polydispersity index (PDI) and zeta potential (ZP) for LOR and LNs.

Sample	LOR (mg)	Stabilizer type	Stabilizer concentration (% w/v)	MPS (nm)	PDI	ZP (mV)
LOR	100	–	–	4607.5 ± 41.7	0.71 ± 0.18	−7.73 ± 5.28
LN1	100	PVP-K25	0.2	4900 ± 71.98	0.98 ± 0.028	−13.4 ± 4.02
LN2	100	HPMC	0.2	4212 ± 14.14	0.767 ± 0.18	−11.9 ± 4.51
LN3	100	SLS	0.2	1496.3 ± 17.457	0.414 ± 0.11	−54 ± 7.75
LN4	100	Tween 80	0.2	414.9 ± 9.02	0.217 ± 0.03	−23 ± 6.51
LN5	100	F68	0.2	246.5 ± 1.83	0.133 ± 0.03	−6.51 ± 3.98
LN6	100	F68	0.4	288.3 ± 37.33	0.104 ± 0.01	−6.36 ± 4.45
LN7	100	F68	0.6	325.4 ± 28.20	0.198 ± 0.01	−12.1 ± 5.91
LN8	100	PVP-K25 + SLS	0.2 + 0.2	589.3 ± 12.66	0.226 ± 0.03	−58.7 ± 8.54
LN9	100	F68 + SLS	0.2 + 0.2	557.4 ± 31.47	0.196 ± 0.03	−67.2 ± 8.14
LN10	50	F68 + PVP-K25	0.2 + 0.2	306.7 ± 14.97	0.158 ± 0.11	−27.8 ± 5.08
LN11	75	F68 + PVP-K25	0.2 + 0.2	276.5 ± 2.69	0.108 ± 0.02	−4.81 ± 4.11
LN12	100	F68 + PVP-K25	0.2 + 0.2	253.4 ± 1.27	0.123 ± 0.01	−11.14 ± 4.89
LN13	100	F68 + PVP-K25	0.2 + 0.4	265.6 ± 20.79	0.122 ± 0.03	−18.10 ± 3.85
LN14	100	F68 + PVP-K25	0.2 + 0.6	307.25 ± 7.28	0.166 ± 0.01	−23.6 ± 5.07
LN15	100	Tween80 + PVP-K25	0.2 + 0.2	423.4 ± 15.06	0.202 ± 0.02	−22.9 ± 4.39

HPMC or PVP-K25 alone as a single stabilizer was insufficient to stabilize LOR nanoparticles. Adding either of these hydrophilic polymers alone yielded high MPS (4900 ± 71.98 and 4212 ± 14.14 nm, respectively) with a large particle size distribution as reflected by the PDI values (0.98 ± 0.028 and 0.767 ± 0.182, respectively). This failure to produce stable nanoparticles can be attributed to the weak adsorption of these polymers onto LOR's surface, as well as to the poor dipole-dipole interaction between LOR and the polymers because of a low polar surface area of LOR (Bartzatt, 2017). SLS alone was also found to be unsuitable to stabilize LNs. SLS-containing LNs were characterized by an MPS of 1496.3 ± 174.57 nm and a PDI of 0.414 ± 0.109, which can be related to the high solubility and insufficient hydrophobicity of SLS, leading to insufficient and incomplete adsorption on LOR's surface (Obeidat and Sallam, 2014). In contrast, Tween 80 and F68 were suitable to produce LNs when they were used on their own. Using Tween 80 and F68 yielded LNs with an MPS of 414.9 ± 9.02 and 246.5 ± 1.38 nm, respectively, with a narrow particle size distribution (PDI was 0.217 ± 0.034 for LNs containing Tween 80 and 0.133 ± 0.03 for those containing F68). Combining SLS with F68 orPVP-K25 augmented the latter one's favourable effects on nanosuspension stabilization, yielding an MPS less than 600 nm, while the combination of Tween 80 or F68 with PVP-K25 did not induce any significant changes compared to Tween 80 or F68 alone. Different concentrations of F68 as single stabilizer yielded different MPSs with increasing diameter as concentration increased, due to a higher viscosity of the solutions, which hinders solvent diffusion and affects the transmission of ultrasonic waves.

Drug concentration had a significant effect on particle size reduction. Using a fixed 1:1 ratio of 0.2% w/v of F68 and PVP-K25 as stabilizers, the smallest MPS was obtained with 100 mg of LOR. This can be explained by supersaturation, which determines the nucleation process. A higher drug concentration led to a higher rate of nucleation, resulting in a large number of nuclei and thus a smaller particle size (Lonare and Patel, 2013).

For stable nanosuspensions, zeta potential has to exceed ± 20 mV and ± 30 mV for sterically and electrically stabilized NSs, respectively (Agrawal and Patel, 2011). The highest zeta potentials were detected for SLS-containing LNs due to the negative charge of this stabilizer compound. However, their MPS and PDI values were unfavourable.

Selecting LNs for further analysis was basically established on their MPS and PDI values as evaluation indices. ZP was not involved, as the subsequent drying procedure could influence of the electro kinetic potential present in nanosuspensions. Thus, although LNs containing F68 or PVP-K25 were characterized by negative zeta potentials between −27.8 ± 5.08 and −4.81 ± 4.11 mV, LNs containing these two stabilizers were selected for further analysis. While Tween 80 also proved to be an efficient stabilizer producing LNs with an acceptable ZP of approximately −23 mV, in this case particle size was higher than that for LNs containing F68 because of a higher solubility of LOR in Tween 80 (2.25 μg/ml and 97.674 μg/ml in 0.2% w/v F68 and Tween 80, respectively).

In summary, LNs suitable for further processing were prepared using the following process parameters: 30 min sonication time, 50% amplitude of sonication power, 4 °C sonication temperature and a solvent: antisolvent ratio of 1:40. Regarding the materials, a drug amount of 100 mg was convenient with superiority for 0.2% w/v F68 either as a single stabilizer or as a mixture with PVP-K25 at 1:1 or 1:2 w: w ratios.

3.4. Effects of freeze-drying on particle size and stability

Aggregation of the selected LNs did not occur for 1 week upon storage at 4 °C, and nanoscale particle size was preserved (Table 3). However, MPS increased for all the selected samples compared to the MPS measured on the day of preparation: for LN5 MPS increased from 246.5 to 276.1 nm, for LN12 MPS increased from 253.4 to 283.4 nm, while for LN13 MPS increased from 265.6 to 294.1 nm. These changes indicate that although particle size remains in the nanosuspension range, a particle size increment of 28.5–30 nm need to be considered over time. This storage time was enough for the nanosuspension to be transferred into the freeze-dryer and converted into dried nanoparticles.

Other LNs were transformed into DLNs. The selected DLNs were easily redistributed to their original volume at nanosized range with accepted PDI (Table 4) and higher ZP than corresponding nanosuspensions, probably due to an enhanced specific interaction between LOR and the polymeric stabilizers during drying and hence stability (Kim and Lee, 2010). The higher ZP could assure the physical stability of DLNs.

3.5. Morphology

The morphology of pure LOR showed an irregular rod-like crystal shape with a particle size above 5 μm with some aggregation, resulting in a broad range of size distribution. In the PMs drug particles clearly

Table 3
Mean particle size (MPS), polydispersity index (PDI) and zeta potential (ZP) for selected LNs after 7 days of storage at 4 °C.

Sample	MPS (nm)	PDI	ZP (mV)
LN5	276.1 ± 17.11	0.137 ± 0.05	−7.8 ± 3.36
LN12	283.4 ± 14.32	0.144 ± 0.02	−17.4 ± 5.23
LN13	294.1 ± 11.61	0.141 ± 0.04	−20.6 ± 7.46

Table 4
Mean particle size (MPS), polydispersity index (PDI) and zeta potential (ZP) for the selected DLNs after reconstitution in water.

Sample	MPS (nm)	PDI	ZP (mV)
DLN5	406.80 ± 16.32	0.240 ± 0.018	−25.80 ± 5.87
DLN12	353.55 ± 31.75	0.195 ± 0.037	−22.35 ± 5.62
DLN13	441.42 ± 37.90	0.246 ± 0.023	−20.70 ± 4.82

aggregated, resulting in large particle sizes. DLNs were characterized by short rod shape particles in the nanorange. The surfaces of DLNs were smooth due to the uniform drug dispersion at the molecular level. SEM images also show some excess crystals appearing on the surface (Fig. 2).

3.6. Structural investigations (XRPD, DSC and FT-IR)

Pure LOR XRPD diffractogram displayed intense crystalline 2θ peaks between 5° and 30°, indicating its crystalline nature. The PMs showed the characteristic crystalline diffraction peaks of LOR, while the characteristic crystalline peaks disappeared in case of DLNs, producing a halo and a diffused pattern typical of an amorphous material (Fig. 3). The values indicating the degree of crystallinity also revealed significant changes of the crystal structure for DLNs. Compared to LOR, DLN5 and DLN12 showed a degree of crystallinity of approximately 37%, while DLN13, characterized by highest level of amorphicity, had a degree of crystallinity of 18.14%. The crystallinity of DLNs containing PVP-K25 decreased to half when the polymer concentration increased two-fold (i.e. DLN12 versus DLN13).·These observations support that the crystalline structure vanishes as a result of the precipitation and drying processes (Colombo et al., 2017).To evaluate the effects of the excipients and freeze-drying on XRPD diffractograms of DLNs, the stabilizers F68 and PVP-K25, as well as their combinations were ultrasonicated and freeze-dried under the same conditions applied for the preparation of DLNs. The XRPD diffractograms for freeze-dried F68 showed the characteristic peaks of F68 (2θ = 19.1° and 23.3°) either alone or in combination with PVP-K25 at 1:1 and 1:2 weight ratios (Fig. 4). However, the signal intensity of F68 peaks were less pronounced on DLNs' diffractograms, and PVP-K25 maintained the amorphous state. These investigations support that the amorphous structure of DLNs, as demonstrated by the diffractograms, is related to the lower level of LOR's crystallinity rather than to the effects of the stabilizers used (Ramos Yacasi et al., 2017).

To evaluate the thermal behavior of the nanoparticles prepared, DSC thermograms of the raw materials, PMs and DLNs were taken (Fig. 4a). Pure LOR exhibited a single sharp endothermic peak at 135.5 °C, corresponding to its melting point. F68 also showed a single peak for its melting point at 55 °C. For PVP-K25, the peak corresponding to the evaporation of water appeared in the temperature range of 50–80 °C (Ruan et al., 2005). The absence of LOR peaks in PMs may be attributed to the effect of F68 as it melted at 55 °C and dissolved LOR during further heating. This hypothesis is supported by the XRPD results, showing that crystalline LOR is present in PMs (Ahuja et al., 2007). DLNs showed two broad peaks, one at 55–60 °C and the other at 110 °C. These thermal events could be related to TRE, to the interactions between the drug, the stabilizer and TRE during freeze-drying, to the phenomenon of the drug's dissolving in the stabilizer or to the transformation into the amorphous state (Chang et al., 2017; Dolenc et al., 2009). DSC thermograms of the ultasonicated, freeze-dried excipients (Fig. 4b) revealed specific interactions between the components of excipient mixtures during freeze-drying. Moreover, a change in the thermogram of TRE in freeze-dried samples containing PVP-K25, i.e. FD-(PVP-K25/TRE) and FD-(F68/PVP-K25/TRE) revealed the

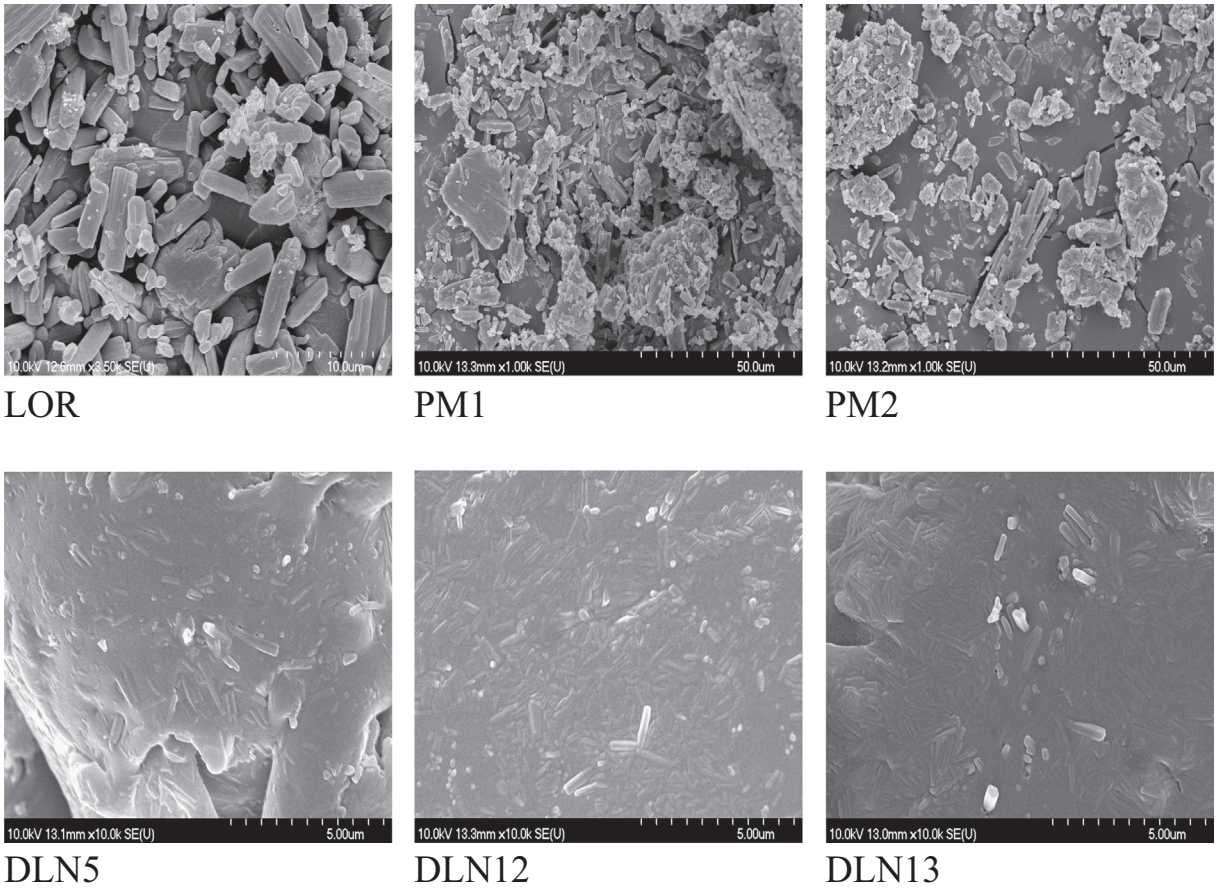

Fig. 2. SEM images of LOR, PM1, PM2, DLN5, DLN12 and DLN13.

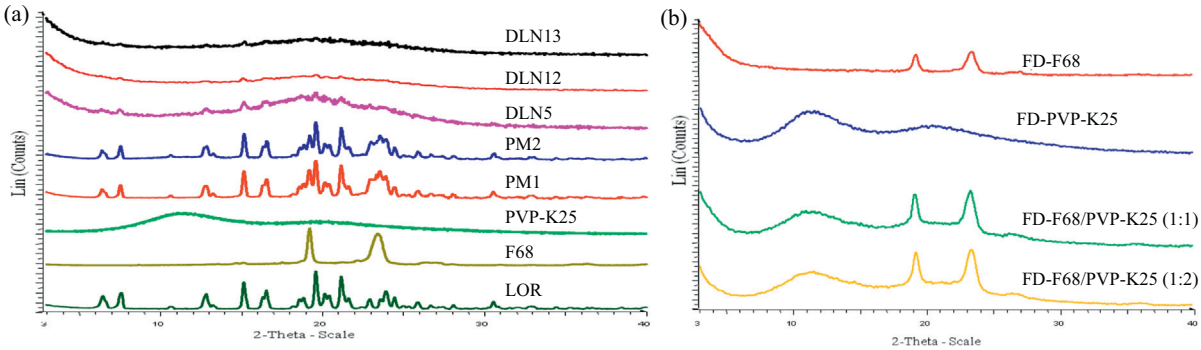

Fig. 3. (a) XRPD diffractograms of LOR, F68, PVP-K25, PM1, PM2, DLN5, DLN12 and DLN13. (b) XRPD diffractograms of FD-F68, FD-PVP-K25, FD-F68/K25 (1:1) and FD-F68/K25 (1:2).

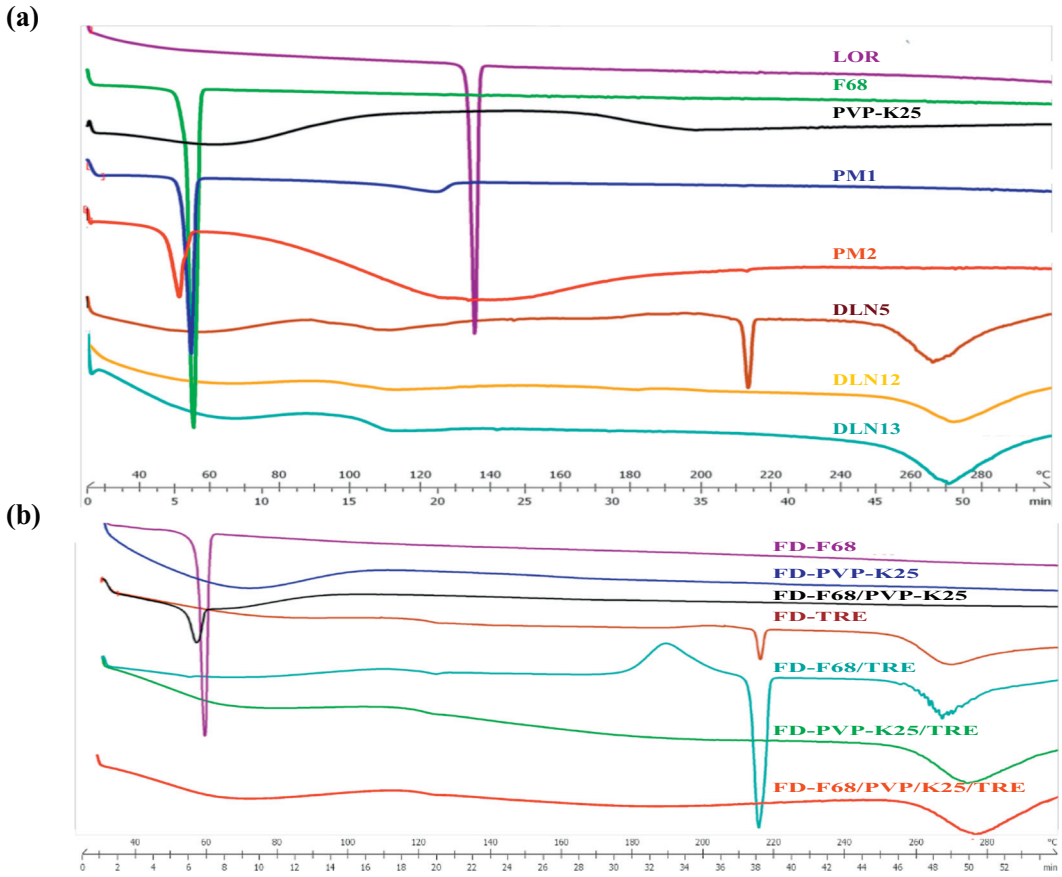

Fig. 4. (a) DSC thermograms of LOR, F68, PVP-k25, PM1, PM2, DLN5, DLN12 and DLN13. (b) DSC thermograms of ultasonicated, freeze-dried excipients; F68, PVP-K25, TRE, F68/PVP-K25, F68/TRE, PVP-K25/TRE and F68/PVP-K25/TRE.

absence of the endothermic peak characteristic of TRE at 210 °C due to interactions (Cardona et al., 1997; Imamura et al., 2008; Taylor, 1998).

FT-IR spectral analysis was performed to study the possibility of molecular interactions between LOR and the stabilizers. The FT-IR spectra of the raw materials and of DLNs are shown in Fig. 5. Pure LOR's FT-IR spectrum is characterized by principal bands at approximately 997 cm^{-1} for Aryl C—Cl stretching and 1227 cm^{-1} for —C—N stretching of aryl N. There are two characteristic bands at 1560 and 1703 cm^{-1} that correspond to C—O bonds of the amide or ester groups. Bands from 3000 to 2850 cm^{-1} correspond to the CH bond. On the other hand, PVP-K25 showed important bands at 3468 cm^{-1} (O—H stretching vibrations), 2954 cm^{-1} (C—H stretching) as well as broad peaks at 1666 cm^{-1} (C═O stretching) and at 1290 cm^{-1} (C—N stretching vibrations). F68 showed peaks at 3503 cm^{-1} (OH stretching), 2889 cm^{-1} (C—H stretching) and 1116 cm^{-1} related to C—O bonds stretching (Lin et al., 2010; Wu et al., 2009; Yu et al., 2011). PMs spectra showed the characteristic peaks of pure LOR, indicating negligible interactions between the API and the excipients. On the other hand, DLNs showed major differences at 3532, 2900–2982, 1700 and 997–1171 cm^{-1}. These alternations maybe related to the stabilizers, i.e. interactions of the excipients with LOR during freeze-drying. To reveal the ambiguity, subtracted curves were generated by subtracting the FT-IR spectra of the excipients including TRE from the spectra of corresponding DLNs and PMs (Fig. 6). The peak for LOR in the subtracted curves of PMs was identical to the peak of pure LOR. However, the subtracted curves of DLNs showed an additional peak at 3532 cm^{-1} related to N—H and a peak at 3100 cm^{-1} which was also related to weak stretching OH bonds. Peak weakening and broadening were observed at 1703 and

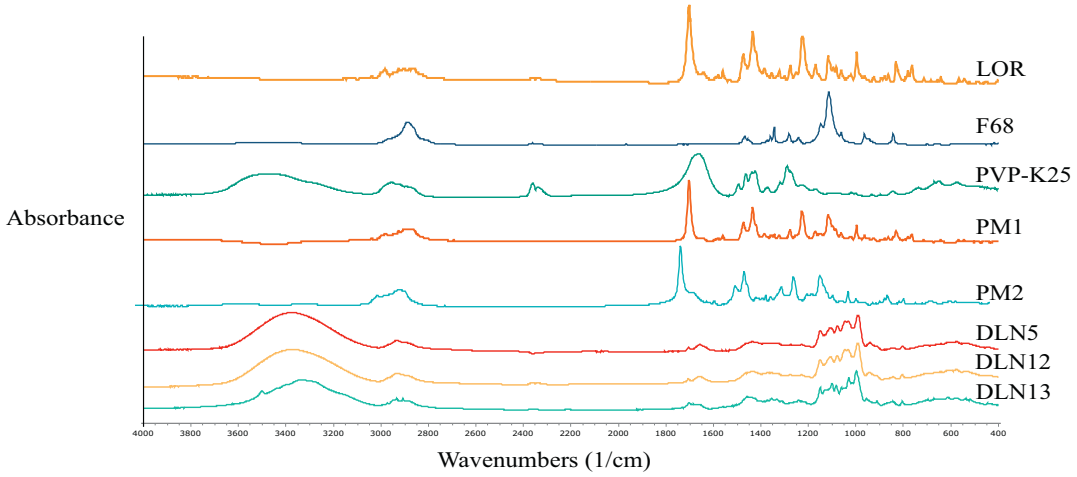

Fig. 5. FT-IR spectra of LOR, F68, PVP-K25, PM1, PM2, DLN5, DLN12 and DLN13.

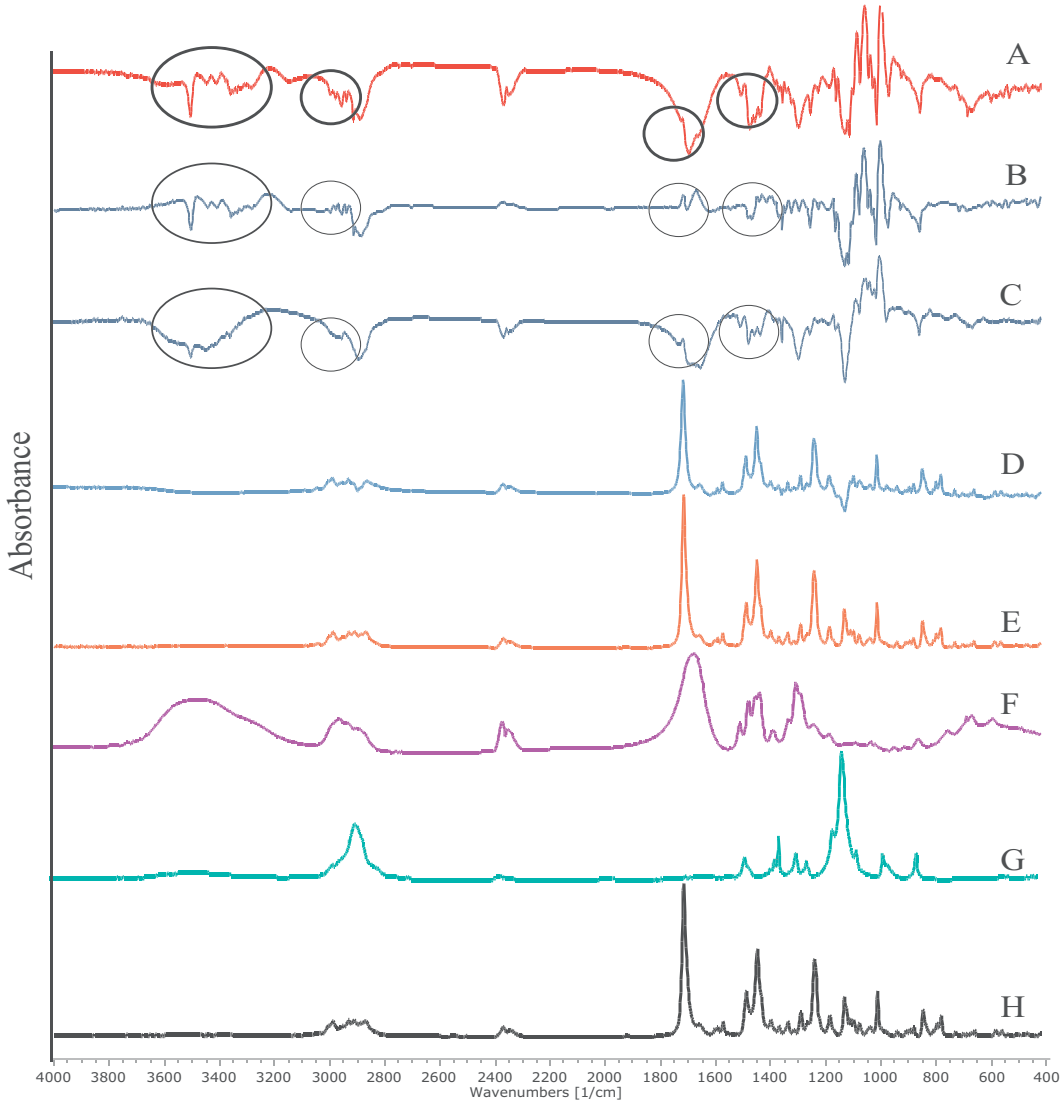

Fig. 6. FT-IR spectra produced by subtracting the FT-IR spectra of the excipients from the spectra of corresponding DLNs and PMs.(A) DLN5-Excipients, (B) DLN12-Excipients, (C) DLN13-Excipients, (D) PM1-Excipients, (E) PM2-Excipients compared to (F) PVP-K25, (G) F68 and (H) LOR.

Table 5
Saturation solubility (μg/ml) of pure LOR and DLNs in distilled water and PBS of pH 7.4.

Sample	Water	PBS of pH 7.4
LOR	2.22 ± 0.001	0.49 ± 0.001
PM1	2.13 ± 0.001	1.87 ± 0.008
PM2	7.06 ± 0.024	4.26 ± 0.011
DLN5	12.17 ± 0.007	4.57 ± 0.063
DLN12	19.11 ± 0.045	3.90 ± 0.008
DLN13	34.26 ± 0.004	4.19 ± 0.001

1500 cm^{-1}. These changes were observed in all DLNs regardless of the type of stabilizers used, indicating that this effect may be attributed to freeze-drying and TRE. These investigations revealed the presence of intermolecular hydrogen bond and dipole-dipole interactions, although no chemical decompositions were detected.

3.7. Solubility and dissolution studies

LOR is characterized by pH-dependent solubility. It has a high solubility at low pH where pyridine nitrogen undergoes protonation. Compared to pure LOR, DLNs showed enhanced saturation solubility in water and in PBS of pH 7.4 (Table 5). Compared to pure LOR, solubility of nanoparticles was increased by approximately 5.5, 8.6 and 15.4-fold for DLN5, DLN12 and DLN13, respectively, in water and 9.3, 8.0 and 8.6-fold for DLN5, DLN12 and DLN13 in PBS of pH 7.4. Water solubility was increased by increasing concentrations of PVP-K25. This may be attributed to the anti-plasticizing activity of PVP-K25, which retards the formation of the crystal lattice.

Based on these solubility data, the sink conditions were not considered. To maintain the sink conditions, saturation solubility of the drug should be at least three times the drug's concentration (Phillips et al., 2012). Moreover, sink conditions applied in dissolution tests lead to rapid dissolution rates for nanosuspensions, hampering the discrimination of the dissolution profiles of different samples (Liu et al., 2013).

Fig. 7 shows the dissolution profiles for LOR, PMs and DLNs at PBS of pH 7.4. Poor dissolution of LOR results in only 6% of the drug dissolving in 120 min. PM1 and PM2 showed higher dissolving of the drug (20.3 and 17.7%, respectively) due to the increased wettability of the drug powder.

DLNs showed higher drug release than pure LOR and PMs. Between 30 and 42% of the drug was detected to be released in the first 10 min, followed by no further significant dissolution because the sink conditions were not applied. Enhanced drug release can be attributed to particle size reduction which produces a higher surface area for dissolution, based on the Noyes-Whitney equation, and possibly to better wettability (Jinno et al., 2006; Noyes and Whitney, 1897). In a careful estimation, DLN5 showed the highest rate of dissolution, which may be related to F68 which forms micelles that increase dissolution. On the other hand, decreasing concentrations of PVP-K25 were found to improve dissolution due to increased viscosity around the stagnant layer. Additionally, the amorphous form is characterized by better solubility compared to the crystalline form (Lindfors et al., 2007).

Table 6
%DE, MDT and $RD_{60\ min}$ for LOR and DLNs.

Sample	%DE30	%DE60	%DE120	MDT	RD_{60min}
LOR	3.309	4.141	5.014	16.439	–
PM1	13.567	17.5671	18.574	6.615	4.243
PM2	8.873	11.797	14.375	16.882	2.849
DLN5	36.662	40.137	43.547	5.0185	9.693
DLN12	27.153	28.726	28.996	0.514	6.937
DLN13	32.876	33.858	33.387	1.218	8.177

The enhancement of dissolution efficiency at different time points and RD_{60} can be noticed as well. MDT values were decreased (Table 6). These experiments demonstrate a higher and faster dissolution of DLNs.

4. Conclusion

LNs and DLNs suitable for further processing were successfully prepared by using 0.2% w/v F68 as a single stabilizer or as a component of a mixture of stabilizers containing 0.2 or 0.4% w/v PVP-K25. Process and material parameters were demonstrated to have a pronounced effect on controlling the properties of the final nanoparticles. Regarding the type(s) of stabilizer(s), two-component mixtures of stabilizers were found to promote a reduction in particle size, as seen in the case of SLS combined with PVP-K25 or F68, whereas this effect was not observed for Tween 80 or F68 combined with PVP-K25. On the other hand, increasing the concentration of F68 above 0.2%w/v resulted in larger particle size. Drug content was also demonstrated to have a considerable effect on MPS. Process parameters of nanosuspension production and drying also affected MPS and ZP of nanoparticles significantly. Time length, power and temperature of the ultrasonication process were confirmed to have a significant effect. Furthermore, we have demonstrated that freeze-drying induces interactions between LOR and the excipients, with TRE behaving as a cryoprotectant compound. Based on our experimental data, we conclude that optimized material and process parameters make it possible to produce dried nanoparticles with MPS and PDI falling in the required range. Moreover, ZPs and the dry state itself guarantee the stability of these nanoparticles. The prepared DLNs exhibited a significant reduction of LOR's crystallinity with enhanced solubility and dissolution compared to the pure drug. Thus, our study supports that is a feasible approach to prepare dried loratadine nanoparticles suitable for designing effective drug preparations, including oral, ophthalmic or nasal dosage forms.

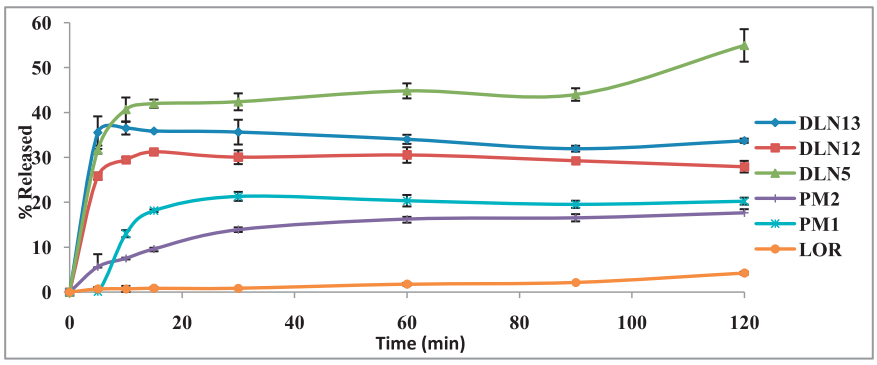

Fig. 7. Dissolution behaviors of LOR, PM1, PM2, DLN5, DLN12 and DLN13 at PBS, pH 7.4.

Declarations of conflicts of interest

The authors report no conflicts of interest related to this work.

Acknowledgement

The experimental work presented in this paper was accomplished with the financial support from a Hungaricum Stipendium grant (2016-2020). The authors thank Dora Bokor, PharmD, for proofreading the manuscript.

References

Abdelwahed, W., Degobert, G., Fessi, H., 2006a. Freeze-drying of nanocapsules: impact of annealing on the drying process. Int. J. Pharm. 324, 74–82. http://dx.doi.org/10.1016/j.ijpharm.2006.06.047.

Abdelwahed, W., Degobert, G., Stainmesse, S., Fessi, H., 2006b. Freeze-drying of nanoparticles: formulation, process and storage considerations. Adv. Drug Deliv. Rev. 58, 1688–1713. http://dx.doi.org/10.1016/j.addr.2006.09.017.

Agrawal, Y., Patel, V., 2011. Nanosuspension: an approach to enhance solubility of drugs. J. Adv. Pharm. Technol. Res. 2, 81. http://dx.doi.org/10.4103/2231-4040.82950.

Ahuja, N., Katare, O.P., Singh, B., 2007. Studies on dissolution enhancement and mathematical modeling of drug release of a poorly water-soluble drug using water-soluble carriers. Eur. J. Pharm. Biopharm. 65, 26–38. http://dx.doi.org/10.1016/j.ejpb.2006.07.007.

Ambrus, R., Kocbek, P., Kristl, J., Šibanc, R., Rajkó, R., Szabó-Révész, P., 2009. Investigation of preparation parameters to improve the dissolution of poorly water-soluble meloxicam. Int. J. Pharm. 381, 153–159. http://dx.doi.org/10.1016/j.ijpharm.2009.07.009.

Anil, P., Pravin, C., Prashant, G., Amol, P., Prakash, B., 2016. Study the effect of surfactant concentration and ultrasonication time on aqueous solubility, particle size and in-vitro drug diffusion of ezogabine nanosuspension by 3 2 factorial designs. Br. Biomed. Bull. 4, 15–26.

Bartos, C., Ambrus, R., Sipos, P., Budai-Szucs, M., Csányi, E., Gáspár, R., Márki, Á., Seres, A.B., Sztojkov-Ivanov, A., Horváth, T., Szabó-Révész, P., 2015a. Study of sodium hyaluronate-based intranasal formulations containing micro- or nanosized meloxicam particles. Int. J. Pharm. 491, 198–207. http://dx.doi.org/10.1016/j.ijpharm.2015.06.046.

Bartos, C., Kukovecz, Á., Ambrus, R., Farkas, G., Radacsi, N., Szabó-Révész, P., 2015b. Comparison of static and dynamic sonication as process intensification for particle size reduction using a factorial design. Chem. Eng. Process. Process Intensif. 87, 26–34. http://dx.doi.org/10.1016/j.cep.2014.10.015.

Bartos, C., Szabó-Révész, P., Bartos, C., Katona, G., Jójárt-Laczkovich, O., Ambrus, R., 2016. The effect of an optimized wet milling technology on the crystallinity, morphology and dissolution properties of micro- and nanonized meloxicam. Molecules 21. http://dx.doi.org/10.3390/molecules21040507.

Bartzatt, R., 2017. Comparative analysis of antihistamines and nonsteroidal anti-inflammatory drugs (NSAIDs): properties, structure and prediction of new potential drugs. J. Adv. Med. Pharm. Sci. 12, 1–18. http://dx.doi.org/10.9734/JAMPS/2017/32695.

Beirowski, J., Inghelbrecht, S., Arien, A., Gieseler, H., 2011. Freeze-drying of nanosuspensions, 1: freezing rate versus formulation design as critical factors to preserve the original particle size distribution. J. Pharm. Sci. 100, 1958–1968. http://dx.doi.org/10.1002/jps.22425.

Cardona, S., Schebor, C., Buera, M.P., Karel, M., Chirife, J., 1997. Thermal stability of invertase in reduced-moisture amorphous matrices in relation to glassy state and trehalose crystallization. J. Food Sci. 62, 105–112. http://dx.doi.org/10.1111/j.1365-2621.1997.tb04378.x.

Chang, R., Fu, Q., Li, Y., Wang, M., Du, W., Chang, C., Zeng, A., 2017. Crystallization and relaxation dynamics of amorphous loratadine under different quench-cooling temperatures. CrystEngComm 19, 335–345. http://dx.doi.org/10.1039/C6CE01645F.

Chen, A., Shi, Y., Yan, Z., Hao, H., Zhang, Y., Zhong, J., Hou, H., 2015. Dosage form developments of nanosuspension drug delivery system for oral administration route. Curr. Pharm. Des. 21, 4355–4365. http://dx.doi.org/10.2174/1381612821666150901105026.

Colombo, M., Orthmann, S., Bellini, M., Staufenbiel, S., Bodmeier, R., 2017. Influence of drug brittleness, nanomilling time, and freeze-drying on the crystallinity of poorly water-soluble drugs and its implications for solubility enhancement. AAPS PharmSciTech 18. http://dx.doi.org/10.1208/s12249-017-0722-4.

Costa, P., Lobo, J.M.S., 2001. Modelling and comparison of dissolution profiles. Eur. J. Pharm. Sci. 13, 123–133. http://dx.doi.org/10.1016/S0928-0987(01)00095-1.

Dagenais, C., Avdeef, A., Tsinman, O., Dudley, A., Beliveau, R., 2009. P-glycoprotein deficient mouse in situ blood-brain barrier permeability and its prediction using an in combo PAMPA model. Eur. J. Pharm. Sci. 38, 121–137. http://dx.doi.org/10.1016/j.ejps.2009.06.009.

Dhumal, R.S., Biradar, S.V., Yamamura, S., Paradkar, A.R., York, P., 2008. Preparation of amorphous cefuroxime axetil nanoparticles by sonoprecipitation for enhancement of bioavailability. Eur. J. Pharm. Biopharm. 70, 109–115. http://dx.doi.org/10.1016/j.ejpb.2008.04.001.

Dolenc, A., Kristl, J., Baumgartner, S., Planinšek, O., 2009. Advantages of celecoxib nanosuspension formulation and transformation into tablets. Int. J. Pharm. 376, 204–212. http://dx.doi.org/10.1016/j.ijpharm.2009.04.038.

Du, J., Li, X., Zhao, H., Zhou, Y., Wang, L., Tian, S., Wang, Y., 2015. Nanosuspensions of poorly water-soluble drugs prepared by bottom-up technologies. Int. J. Pharm. 495, 738–749. http://dx.doi.org/10.1016/j.ijpharm.2015.09.021.

Frizon, F., Eloy, J. de O., Donaduzzi, C.M., Mitsui, M.L., Marchetti, J.M., 2013. Dissolution rate enhancement of loratadine in polyvinylpyrrolidone K-30 solid dispersions by solvent methods. Powder Technol. 235, 532–539. http://dx.doi.org/10.1016/j.powtec.2012.10.019.

Han, M.Z.I.K., Aus, D.R., Filipovi, P., 2004. Classification of loratadine based on the biopharmaceutics drug classification concept and possible in vitro – in vivo correlation. Biol. Pharm. Bull. 27, 1630–1635. http://dx.doi.org/10.1248/bpb.27.1630.

Hao, J., Gao, Y., Zhao, J., Zhang, J., Li, Q., Zhao, Z., Liu, J., 2015. Preparation and optimization of resveratrol nanosuspensions by antisolvent precipitation using Box-Behnken design. AAPS PharmSciTech 16, 118–128. http://dx.doi.org/10.1208/s12249-014-0211-y.

Hin Teng, L.H., Raja Kumar, J., Leng, L., Selvi, M.V.R.A., 2015. Nanoparticle loaded thermosensitive nasal in-situ gels for delivery of loratadine: in-vitro & in-vivo evaluation studies. Rapp. Pharm. 1, 17–27.

Imamura, K., Asaimo, Y., Maruyama, Y., Yokoyama, T., Nomura, M., Ogawa, S., Nakanishi, K., 2008. Characteristics of hydrogen bond formation between sugar and polymer in freeze-dried mixtures under different rehumidification conditions and its impact on the glass transition temperature. J. Pharm. Sci. 97, 1301–1312. http://dx.doi.org/10.1002/jps.21066.

Iurian, S., Bogdan, C., Tomuță, I., Szabó-Révész, P., Chvatal, A., Leucuța, S.E., Moldovan, M., Ambrus, R., 2017. Development of oral lyophilisates containing meloxicam nanocrystals using QbD approach. Eur. J. Pharm. Sci. 104, 356–365. http://dx.doi.org/10.1016/j.ejps.2017.04.011.

Jiang, T., Han, N., Zhao, B., Xie, Y., Wang, S., 2012. Enhanced dissolution rate and oral bioavailability of simvastatin nanocrystal prepared by sonoprecipitation. Drug Dev. Ind. Pharm. 38, 1230–1239. http://dx.doi.org/10.3109/03639045.2011.645830.

Jinno, J.I., Kamada, N., Miyake, M., Yamada, K., Mukai, T., Odomi, M., Toguchi, H., Liversidge, G.G., Higaki, K., Kimura, T., 2006. Effect of particle size reduction on dissolution and oral absorption of a poorly water-soluble drug, cilostazol, in beagle dogs. J. Control. Release 111, 56–64. http://dx.doi.org/10.1016/j.jconrel.2005.11.013.

Khan, K.A., 1975. The concept of dissolution efficiency. J. Pharm. Pharmacol. 27, 48–49. http://dx.doi.org/10.1111/j.2042-7158.1975.tb09378.x.

Kim, S., Lee, J., 2010. Effective polymeric dispersants for vacuum, convection and freeze drying of drug nanosuspensions. Int. J. Pharm. 397, 218–224. http://dx.doi.org/10.1016/j.ijpharm.2010.07.010.

Li, H., Tan, Y., Yang, L., Gao, L., Wang, T., Yang, X., Quan, D., 2015. Dissolution evaluation in vitro and bioavailability in vivo of self-microemulsifying drug delivery systems for pH-sensitive drug loratadine. J. Microencapsul. 32, 175–180. http://dx.doi.org/10.3109/02652048.2014.985340.

Lin, S.Y., Hsu, C.H., Sheu, M.T., 2010. Curve-fitting FTIR studies of loratadine/hydroxypropyl-β-cyclodextrin inclusion complex induced by co-grinding process. J. Pharm. Biomed. Anal. 53, 799–803. http://dx.doi.org/10.1016/j.jpba.2010.06.010.

Lindfors, L., Skantze, P., Skantze, U., Westergren, J., Olsson, U., 2007. Amorphous drug nanosuspensions. 3. Particle dissolution and crystal growth. Langmuir 23, 9866–9874. http://dx.doi.org/10.1021/la700811b.

Liu, D., Xu, H., Tian, B., Yuan, K., Pan, H., Ma, S., Yang, X., Pan, W., 2012. Fabrication of Carvedilol Nanosuspensions Through the Anti-solvent Precipitation–Ultrasonication Method for the Improvement of Dissolution Rate and Oral Bioavailability. http://dx.doi.org/10.1208/s12249-011-9750-7.

Liu, P., De Wulf, O., Laru, J., Heikkilä, T., van Veen, B., Kiesvaara, J., Hirvonen, J., Peltonen, L., Laaksonen, T., 2013. Dissolution studies of poorly soluble drug nanosuspensions in non-sink conditions. AAPS PharmSciTech 14, 748–756. http://dx.doi.org/10.1208/s12249-013-9960-2.

Lonare, A.A., Patel, S.R., 2013. Antisolvent crystallization of poorly water soluble drugs. Int. J. Chem. Eng. Appl. 4, 337–341. http://dx.doi.org/10.7763/IJCEA.2013.V4.321.

Matteucci, M.E., Hotze, M.A., Johnston, K.P., Williams, R.O., 2006. Drug nanoparticles by antisolvent precipitation: mixing energy versus surfactant stabilization. Langmuir 22, 8951–8959. http://dx.doi.org/10.1021/la061122t.

Merisko-Liversidge, E.M., Liversidge, G.G., 2008. Drug nanoparticles: formulating poorly water-soluble compounds. Toxicol. Pathol. 36, 43–48. http://dx.doi.org/10.1177/0192623307310946.

Mishra, B., Sahoo, J., Dixit, P.K., 2015. Formulation and process optimization of naproxen nanosuspensions stabilized by hydroxy propyl methyl cellulose. Carbohydr. Polym. 127, 300–308. http://dx.doi.org/10.1016/j.carbpol.2015.03.077.

Moore, K., Haroz, R., 2016. When hydromorphone is not working, try loratadine: an emergency department case of loratadine as abortive therapy for severe pegfilgrastim-induced bone pain. J. Emerg. Med. 1–3. http://dx.doi.org/10.1016/j.jemermed.2016.08.018.

Möschwitzer, J., 2010. Nanotechnology: particle size reduction technologies in the pharmaceutical development process. Am. Pharm. Rev. 54–59.

Müller, R.H., Gohla, S., Keck, C.M., 2011. State of the art of nanocrystals - special features, production, nanotoxicology aspects and intracellular delivery. Eur. J. Pharm. Biopharm. 78, 1–9. http://dx.doi.org/10.1016/j.ejpb.2011.01.007.

Nacsa, Á., Ambrus, R., Berkesi, O., Szabó-Révész, P., Aigner, Z., 2008. Water-soluble loratadine inclusion complex: analytical control of the preparation by microwave irradiation. J. Pharm. Biomed. Anal. 48, 1020–1023. http://dx.doi.org/10.1016/j.jpba.2008.07.001.

Nacsa, Á., Berkesi, O., Szabó-Révész, P., Aigner, Z., 2009. Achievement of pH-independence of poorly-soluble, ionizable loratadine by inclusion complex formation with dimethyl-ß-cyclodextrin. J. Incl. Phenom. Macrocycl. Chem. 64, 249–254. http://dx.doi.org/10.1007/s10847-009-9558-1.

Noyes, A.A., Whitney, W.R., 1897. The rate of solution of solid substances in their own

solutions. J. Am. Chem. Soc. 19, 930–934. http://dx.doi.org/10.1021/ja02086a003.
Obeidat, W.M., Sallam, A.-S.A., 2014. Evaluation of Tadalafil nanosuspensions and their PEG solid dispersion matrices for enhancing its dissolution properties. AAPS PharmSciTech 15, 364–374. http://dx.doi.org/10.1208/s12249-013-0070-y.
Patravale, V.B., Date, A. a, Kulkarni, R.M., 2004. Nanosuspensions: a promising drug delivery strategy. J. Pharm. Pharmacol. 56, 827–840. http://dx.doi.org/10.1211/0022357023691.
Pawar, V.K., Singh, Y., Meher, J.G., Gupta, S., Chourasia, M.K., 2014. Engineered nanocrystal technology: in-vivo fate, targeting and applications in drug delivery. J. Control. Release 183, 51–66. http://dx.doi.org/10.1016/j.jconrel.2014.03.030.
Phillips, D.J., Pygall, S.R., Cooper, V.B., Mann, J.C., 2012. Overcoming sink limitations in dissolution testing: a review of traditional methods and the potential utility of biphasic systems. J. Pharm. Pharmacol. 64, 1549–1559. http://dx.doi.org/10.1111/j.2042-7158.2012.01523.x.
Popović, G., Čakar, M., Agbaba, D., 2009. Acid-base equilibria and solubility of loratadine and desloratadine in water and micellar media. J. Pharm. Biomed. Anal. 49, 42–47. http://dx.doi.org/10.1016/j.jpba.2008.09.043.
Quintanar-Guerrero, D., Ganem-Quintanar, A., Allémann, E., Fessi, H., Doelker, E., 1998. Influence of the stabilizer coating layer on the purification and freeze-drying of poly (D,L-lactic acid) nanoparticles prepared by an emulsion-diffusion technique. J. Microencapsul. 15, 107–119. http://dx.doi.org/10.3109/02652049809006840.
Rabinow, B.E., 2004. Nanosuspensions in drug delivery. Nat. Rev. Drug Discov. 3, 785–796. http://dx.doi.org/10.1038/nrd1494.
Rahim, H., Sadiq, A., Khan, S., Khan, M.A., Shah, S.M.H., Hussain, Z., Ullah, R., Shahat, A., Ibrahim, K., 2017. Aceclofenac nanocrystals with enhanced in vitro, in vivo performance: formulation optimization, characterization, analgesic and acute toxicity studies. Drug Des. Devel. Ther. Volume 11, 2443–2452. http://dx.doi.org/10.2147/DDDT.S140626.
Ramos Yacasi, G.R., Calpena Campmany, A.C., Egea Gras, M.A., Espina García, M., García López, M.L., 2017. Freeze drying optimization of polymeric nanoparticles for ocular flurbiprofen delivery: effect of protectant agents and critical process parameters on long-term stability. Drug Dev. Ind. Pharm. 43, 637–651. http://dx.doi.org/10.1080/03639045.2016.1275669.
Romeo, C., Li, Q., Copeland, L., 2015. Severe pegfilgrastim-induced bone pain completely alleviated with loratadine: a case report. J. Oncol. Pharm. Pract. 21, 301–304. http://dx.doi.org/10.1177/1078155214527858.
Ruan, L.P., Yu, B.Y., Fu, G.M., Zhu, D.N., 2005. Improving the solubility of ampelopsin by solid dispersions and inclusion complexes. J. Pharm. Biomed. Anal. 38, 457–464. http://dx.doi.org/10.1016/j.jpba.2005.01.030.
Taylor, L.S., 1998. Sugar-polymer hydrogen bond interactions in lyophilized amorphous mixtures. J. Pharm. Sci. 87, 1615–1621. http://dx.doi.org/10.1021/js9800174.
Van Eerdenbrugh, B., Van den Mooter, G., Augustijns, P., 2008. Top-down production of drug nanocrystals: Nanosuspension stabilization, miniaturization and transformation into solid products. Int. J. Pharm. 364, 64–75. http://dx.doi.org/10.1016/j.ijpharm.2008.07.023.
Vyshnavi, V., Indira, S., Prathima, S., 2015. Formulation and evaluation of nasal niosomal in situ gels of loratadine. Int. J. Pharm. Sci. Drug Res. 7, 13–21.
Wu, K., Li, J., Wang, W., Winstead, D.A., 2009. Formation and characterization of solid dispersions of piroxicam and polyvinylpyrrolidone using spray drying and precipitation with compressed antisolvent. J. Pharm. Sci. 98, 2422–2431. http://dx.doi.org/10.1002/jps.21598.
Wu, L., Zhang, J., Watanabe, W., 2011. Physical and chemical stability of drug nanoparticles. Adv. Drug Deliv. Rev. 63, 456–469. http://dx.doi.org/10.1016/j.addr.2011.02.001.
Wu, T.Y., Guo, N., Teh, C.Y., Hay, J.X.W., 2013. Advances in Ultrasound Technology for Environmental Remediation. http://dx.doi.org/10.1007/978-94-007-5533-8.
Xia, D., Quan, P., Piao, H., Piao, H., Sun, S., Yin, Y., Cui, F., 2010. Preparation of stable nitrendipine nanosuspensions using the precipitation-ultrasonication method for enhancement of dissolution and oral bioavailability. Eur. J. Pharm. Sci. 40, 325–334. http://dx.doi.org/10.1016/j.ejps.2010.04.006.
Yu, M., Sun, L., Li, W., Lan, Z., Li, B., Tan, L., Li, M., Yang, X., 2011. Investigation of structure and dissolution properties of a solid dispersion of lansoprazole in polyvinylpyrrolidone. J. Mol. Struct. 1005, 70–77. http://dx.doi.org/10.1016/j.molstruc.2011.08.019.
Zhang, X., Xia, Q., Gu, N., 2006. Preparation of all-trans retinoic acid nanosuspensions using a modified precipitation method. Drug Dev. Ind. Pharm. 32, 857–863. http://dx.doi.org/10.1080/03639040500534184.